Program Digest, 2019 IEEE International Ultrasonics Symposium (IUS)
Glasgow, Scotland, October 6-9, 2019

Ultrasound echo and Photoacoustic Strain Tensor Imaging for In Vivo Observations of Soft Tissue Motion and Blood Flow

Chikayoshi Sumi
Dept of Info & Commun Sci
Sophia University
Tokyo Japan
c-sumi@sophia.ac.jp

***Abstract*—With ultrasound (US) echo and/or photoacoustic (PA) signals, in addition to a high accuracy vectorial Doppler imaging, a high accuracy strain (rate) tensor imaging is performed for both wrist soft tissues and the surrounding bloods. Automatic detection regarding the boundary between a blood vessel and a blood flow region using high intensity PA signals generated at the blood flow positions adjacent to the vessel. Using the detection method instead of a clutter rejection filter, the flow region is successfully detected. Simultaneous imaging of the soft tissues and bloods is also performed.**

Keywords—photoacoustic Doppler, ultrasound echo Doppler, strain tensor, displacement vector, 2D autocorrelation method, median filter

I. INTRODUCTION

We have been developing high accuracy ultrasonic (US)-echo-based Doppler observation methods of a human *in vivo* tissue displacement, velocity or acceleration vector, and a strain or strain rate tensor [1-10, etc]. These methods provide us with clinically simple observation techniques, i.e., only attachment of a probe onto a surface of target regardless the direction of target motion. Recently, we started to observe the mechanical quantities based on photoacoustic imaging (PAI) and last year, we reported the observations of axial strain for human *in vivo* superficial wrist tissues [11,12]. The tissue dynamics generated by a pulsation and a compression/removal of the compression were observed. As known, only a few *in vivo* PAIs have been performed for observing a soft tissue strain [13] and no *in vivo* for a blood flow [14,15].

In this report, in addition to the high accuracy displacement or velocity vector imaging [16], the high accuracy strain or strain rate tensor imaging is performed for both wrist soft tissues and the surrounding bloods. In addition to the differences of frequencies of tissues, we are investigating those of bandwidths for differentiations of tissues [11,12]. With markers or not, PA signals are generated inherently to the respective tissues and then, PA signals enable us to select an target tissue to be imaged. Alternatively, we had been proposing to simultaneously image various tissues in an US-echo mode. For instance, in [11,12], the soft tissue motion and the blood flow were imaged simultaneously in addition to those obtained from PA signals.

In [11], the 2-dimensional (2D) cross-spectrum phase gradient method (CSPGM) [1] was used. The method is robust to noises [3]. In [12], the 2D autocorrelation method (AM) [2-6] was used. The method requires less calculations than the CSPGM and yields a high accuracy measurement particularly when the signals have a high signal-to-noise ratio (SNR) [3]. As known, almost the PA signals have a lower SNR than the US echo signals, which results in a lower accuracy measurement than the echo Doppler. Since the echo Doppler also yields a low accuracy measurement when the echo SNR is low, we previously proposed to perform the median filtering on a coarse estimate to be obtained by the multidimensional cross-correlation method (CCM) or CSPGM [17], which is used for a fine estimation performed by CSPGM or AM. In this report, the median filtering is used for the PA Doppler measurement.

II. METHODS

A commercial PAI system, AcousticX (CYBERDYNE, Inc., Japan), was used. The volunteer was 54-years-old male. Via a water bag (10 mm depth), plane waves of an LED light (850nm, totally 400 μJ) and an ultrasound (a linear-array type with a nominal freq., 7 MHz) were interchangeably transmitted to his superficial wrist tissues. Generated US echo and PA frame rates were 15.4 Hz. By performing a reception dynamic focusing using our developed Fourier beamforming methods [18], the lateral modulations (LMs) [2-6] with crossed beams ($\pm$ 10 degrees) and the nonsteered single beams [2,6] were respectively generated over the ROI (40 mm depth). For a 2D displacement vector measurement, the 2D AM [2-6] was used with the median filter.

For the automatic differentiations between the arterial blood and the surrounding soft tissues, the blood flow positions adjacent to the blood vessel were estimated by detecting large PA intensity changes along the depth direction.

Here, P(I,J) expresses enveloped PA signals. When a blood vessel runs in a lateral direction (J) being parallel to the target surface, the boundaries between anterior and posterior

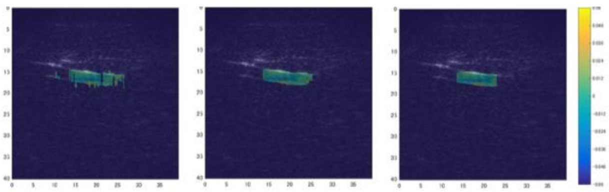

(a) (b) (c)

Fig. 1. Images of blood lateral displacements (velocities) observed with PA lateral modulation. (a) No median filtering and median filtering with (a) 33 and (c) 97 data.

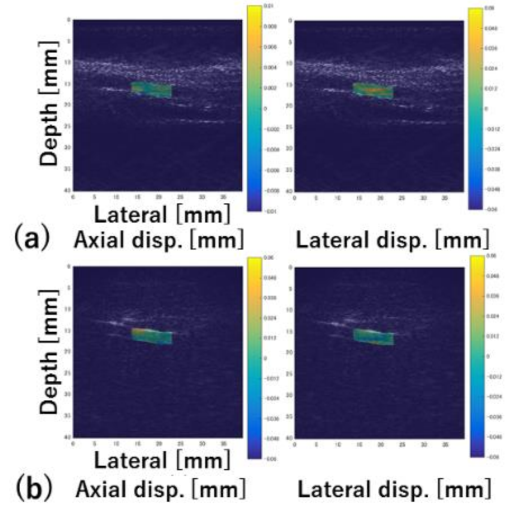

Fig. 2. Blood flow images. (a) rf-echo and (b) PA.

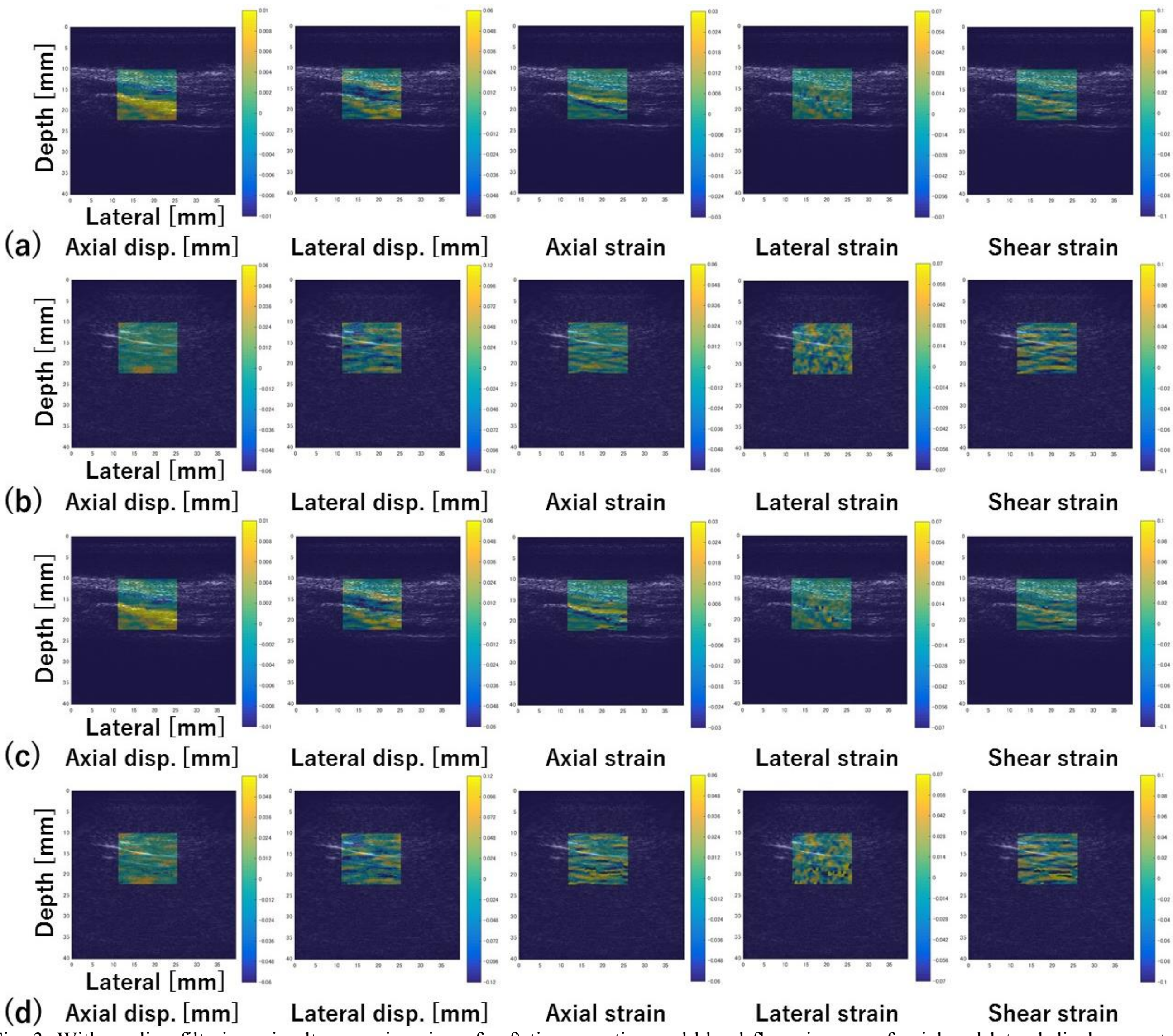

Fig. 3. With median filtering, simultaneous imaging of soft tissue motion and blood flow: images of axial and lateral displacements (velocities), and axial, lateral and shear strains (strain rates) measured from (a) US echo and (b) next PA signals generated by reception beamforming in axial direction. (c) and (d) With no median filtering, images corresponding to (a) and (b).

vessels and blood flow region were able to be confirmed by detecting the positions where the following equations hold:

for the anterior vessel, I increasing,

$$(P(I+1,J)^N - P(I,J)^N) > \text{Threshold, Th1};$$

and for posterior vessel, I decreasing,

$$(P(I\text{-}1,J)^N - P(I,J)^N) > \text{Th2}. \qquad (1)$$

Setting N largely enabled us to determine thresholds simply. Since the boundary was estimated discontinuously, to remove the estimation errors, the median filter was used. This new detection method can be applied to an arbitrary direction of the boundary. A clutter filtering can also be used for an arbitrary direction flow and the detection accuracy is high. However, it is difficult to differentiate tissues with slow motions. In the near future, the combination of the new detection method and the clutter filtering will be performed. Equation (1) corresponds to the 1st order differentiation; and the higher order differentiations can also be used if necessary.

Thus, similarly to the color Doppler or Elastography, the blood flow and the soft tissue motion/deformation measured from US echo or PA data were independently imaged with the corresponding US echo and PA images (video data). As mentioned above, simultaneous imaging of the soft tissues and blood was also performed (video).

III. Experimental Results

Figure 1 shows in the PA lateral modulation case the effectiveness of median filtering for the automatic detection of boundaries between the arterial vessel and the arterial flow region. In eq. (1), N = 3, Th1 = 50,000 and Th2 = 8,000 were set. As shown in Figs. 1b and 1c, the obvious estimation errors shown in Fig. 1a generated with no median filtering are removed with the median filter width of 33 and 97 data. Setting a longer filter width to more stabilize the estimation, the lateral region and lateral resolution decreased. However, the iterative implementations of a properly short filter coped with the problems (omitted).

Figure 2 shows in the non-steered cases the snapshots of axial and lateral blood displacements (velocities) measured from (a) rf-echo and (b) PA signals (33 data). The automatic differentiations based on a PA intensity difference are successfully performed.

And, Fig. 3 shows the snapshots of simultaneous imaging of soft tissues and bloods obtained with the median filtering from the nonsteered (a) rf-echo and (b) PA signals, i.e., the axial and lateral displacements, and axial, lateral and shear strains. Due to the difference in a signal SNR, the results obtained from echo data are more accurate than those obtained from PA data. Figures 2c and 2d respectively show the results with no median filtering for Figs. 2a and 2b. The effectiveness of median filtering can be confirmed by comparing Figs. 2a with 2c, and 2b with 2d. Figures 2a and 2b are respectively more stable than Figs. 2c and 2d, particularly on strain measurements and PA measurements.

Various dynamic data were obtained, e.g., shear phenomena at the vessel walls [16]. The corresponding video data will be shown elsewhere. Although the LM usually performed better than the nonsteered case, a large element pitch resulted in almost the same accuracy (omitted).

IV. Conclusions

The human *in vivo* wrist tissue motion/deformation and blood flow were successfully imaged independently and simultaneously. In addition to the displacement vector (velocity vector), the strain tensor (strain rate tensor) was imaged. For the independent imaging, the automatic detection using the PA signal intensity change for the boundary between the blood vessel and the blood flow region was effective. For the simultaneous imaging, different colors will also be used for a soft tissue motion and a blood flow. For both the automatic detection and the measurement of dynamics, the median filtering was effective. Recently, we enabled us to performed various optimizations even when performing the phase matching [10] such as the regularization [9], the maximum a posteriori estimation [10], etc. Such optimizations will also be performed for these measurements. Overdetermined systems can also be generated by using more beams/waves [7,10] or spectral divisions [8,10] for the respective echo and PA data; and for both echo and PA data (a mixed case).

In the practical applications of rf-echo and PA vectorial Dopplers, such mechanical quantities can be respectively imaged in a real time; and the quantities measured from rf-echo and PA data can also be imaged interchangeably and/or in a slow motion mode since they have more information about the tissue dynamics than the past color Doppler or Elastography. In the near future, the results obtained for an arteriosclerosis, a thrombus, a malignant or cancerous lesion and a fatty tissue, etc. will be reported. With the measurements, reconstructions about elasticity, visco-elasticity, viscosity and an internal tissue pressure will also be reported (e.g., [19,20]).

References

[1] C. Sumi, “Fine elasticity imaging on utilizing the iterative rf-echo phase matching method,” IEEE Trans. Ultrason., Ferroelect., Freq. Contr., vol. 46, pp. 158–166, 1999.

[2] C. Sumi, “Digital measurement method of tissue displacement vector from instantaneous phase of ultrasonic echo signal,” Technical report of Jpn. Soc. of Ultrason. in Med., pp. 37–40, Dec. 2002.

[3] C. Sumi, Displacement vector measurement using instantaneous ultrasound signal phase—Multidimensional autocorrelation and Doppler methods,” IEEE Trans UFFC, vol. 55, 24-43, 2008.

[4] C. Sumi, T. Noro, A. Tanuma, “Effective lateral modulations with applications to shear modulus reconstruction using displacement vector measurement,” IEEE Trans UFFC, vol. 55, pp. 2607-2625, 2008.

[5] C. Sumi, Y. Takanashi, K. Ichimaru, “Consideration of generated beam angles increases the accuracy of ultrasonic displacement measurements,” Reports in Medical Imaging, vol. 5, pp. 23-50, 2012.

[6] C. Sumi, Y. Ishii, “Ultrasonic lateral modulation imaging, speckle reduction, and displacement vector measurements using simple single-beam scanning or plural crossed-beam scanning with new spectra frequency division processing methods,” Reports in Medical Imaging, vol. 5, pp. 57-101, 2012.

[7] C. Sumi, “Accuracy comparison of axial and lateral strain measurements achieved using plural steered beams and plane waves and super-resolution imaging,” Proc. Int. Tissue Elasticity Conf., ID: 40, 2015; and Full paper version, 2015.

[8] C. Sumi, “Plural spectral frequency divisions for ultrasonic tissue displacement vector measurement,” Proc of 38th Int Conf IEEE EMBS, pp. 2859-2864, 2016.

[9] C. Sumi, K. Sato, “Regularization for ultrasonic measurements of tissue

displacement vector and strain tensor," IEEE Trans UFFC, vol. 55, pp. 787-799, 2008.

[10] C. Sumi, "New phase matching method for ultrasonic tissue displacement and strain measurements -Application of maximum likelihood and maximum *a posteriori* to multidimensional autocorrelation method," Japanese Journal of Applied Physics, vol. 57, 07LF24, 2018.

[11] C. Sumi, N. Sato, "Photoacoustic strain imaging on human in vivo wrist," Proc of 40th Int Conf IEEE EMBS, 2018.

[12] C. Sumi, N. Sato, "Primary experiment for photoacoustic human in vivo tissue strain imaging," 39th Symp UltraSonic Electronics (USE), ID: 2P5-18, 2018.

[13] P. Hai, Y. Zhou, L. Gong, L. V. Wang, Quantitative photoacoustic elastography in humans, Journal of Biomedcal Optics, 2016, 21(6): 066011.

[14] P. J. van den Berg, K. Daoudi, W. Steenbergen, Photoacoustics **3**, 89 (2015).

[15] J. Brunker, P. Beard, Proc. SPIE **9708**, 97080R-1 (2016).

[16] C. Sumi, "Ultrasound echo and photoacoustic vectorial Doppler tissue motion and blood flow imaging," Proc of 41th Int Conf IEEE EMBS, 2019.

[17] C. Sumi, A. Suzuki, K. Nakayama, "Phantom experiment on estimation of shear modulus distribution in soft tissue from ultrasonic measurement of displacement vector field," IEICE Trans. on Fundamental, vol. E78-A, no. 12, pp. 1655-1664, December 1995.

[18] C. Sumi, "Preliminary experiments of 3-dimensional Fourier beamforming with no approximate interpolation for wavenumber matching." Proc of IEEE Int Ultrasonics Symp, 2018.

[19] C. Sumi, IEEE Trans. Ultrason. Ferroelectr. Freq. Control **55**, 2607 (2008).

[20] C. Sumi, H. Matsuzawa, J Med Ultrasonics **34**, 171 (2007).